Renewable and Sustainable Energy Reviews 37 (2014) 36–46

Contents lists available at ScienceDirect

Renewable and Sustainable Energy Reviews

journal homepage: www.elsevier.com/locate/rser

Potential solar thermal integration in Spanish combined cycle gas turbines

J. Antonanzas [a], E. Jimenez [b], J. Blanco [c], F. Antonanzas-Torres [a,*]

[a] EDMANS Group, Department of Mechanical Engineering, University of La Rioja, Logroño, Spain
[b] Department of Electrical Engineering, University of La Rioja, Logroño, Spain
[c] Department of Mechanical Engineering, University of La Rioja, Logroño, Spain

A R T I C L E I N F O

Article history:
Received 25 November 2013
Received in revised form
14 April 2014
Accepted 3 May 2014
Available online 26 May 2014

Keywords:
CSP
Combined cycle gas turbine
Solar thermal
ISCC

A B S T R A C T

Combined cycle gas turbines (CCGTs) are volumetric machines, which means that their net power output decreases at air temperatures above the design point. Such temperatures generally occur during periods of high solar irradiation. Many countries where these conditions occur, including Spain, have installed a significant number of CCGTs in recent years, with the subsequent yield losses in the summer. This implies enormous potential for solar hybridization, increasing production in peak hours and overall efficiency and reducing CO_2 emissions.

This paper analyzes the overall potential for solar thermal integration in 51 CCGTS (25,340 MW) in mainland Spain under different operating scenarios based on increasing yield, solar fraction and the hourly operational range adapted to the Spanish electricity market, considering actual meteorological conditions.

A production model for integrating solar energy into combined cycles is proposed and described and the code in R is freely released so that the assessment can be replicated.

Contents

1. Introduction . . . 37
2. Data . . . 38
   2.1. CCGT data. . . . 38
   2.2. Meteorological data . . . 38
3. Methodology . . . 38
   3.1. Production model . . . 39
      3.1.1. CCGT analysis . . . 39
      3.1.2. Solar field analysis . . . 40
   3.2. Scenarios of operation . . . 41
      3.2.1. Scenario 0. . . . 41
      3.2.2. Scenario 1. . . . 41
      3.2.3. Scenario 2. . . . 41
      3.2.4. Scenario 3. . . . 41
      3.2.5. Scenario 4. . . . 42
      3.2.6. Scenario 5. . . . 42
   3.3. Software . . . 42
4. Results and discussion. . . . 43
   4.1. Local analysis . . . 43
   4.2. Total analysis . . . 44
5. Conclusions . . . 44

* Corresponding author.
E-mail address: antonanzas.fernando@gmail.com (F. Antonanzas-Torres).

http://dx.doi.org/10.1016/j.rser.2014.05.006
1364-0321/

Acknowledgments . . . 46
References . . . 46

1. Introduction

Solar thermal energy has become a very attractive source of energy as a result of the rise in fossil fuel prices, external energy dependency on politically unstable countries and increased environmental awareness in some societies. Various concentrated solar thermal power technologies (CSP) have arisen such as tower plants, Fresnel and parabolic troughs with different heat transfer fluids (thermal oils, water, air, molten salts, etc.) [1,2]. However, the greatest growth has been in CSP technology based on parabolic troughs with thermal oil as the heat transfer fluid (PT-HTF) [3]. This technology has been operational since the 1980s, linked to the nine Solar Energy Generating Systems (SEGS) developed by Luz Solar International in the USA from 1982 to 1991. After a 15-year gap in which no CSP was developed, PT-HTF has spread since 2008, and its global installed capacity at the end of 2012 stood at 2.55 GW [4]. As a result of the learning curve of PT-HTF, mainly due to the cost reduction in solar field components, capital costs have decreased remarkably [4,5].

Nowadays, there is an increasing interest in improving efficiency in electricity production in combined cycle gas turbines (CCGTs). As a result of the volumetric machine behavior of gas turbines, a significant yield loss occurs at high air temperatures (first-order factor) and under conditions of low relative humidity and low pressure (second-order factors), with the consequent financial losses. The concept of integrating solar thermal energy in CCGT (ISCC) involves a relatively new technology, with a global solar installed capacity of about 200 MW [6], which has been operational since 2010, as shown in Table 1. In addition, two other ISCCs are under construction, the Agua Prieta II ISCC (Mexico, 464 MW CCGT, 14 MW solar) and the Ningxia ISCC (China, 92 MW). ISCCs take advantage of the fact that higher air temperatures are also associated with periods of higher direct normal solar irradiation. ISCCs have other technical advantages, such as a greater thermo-dynamical efficiency (fossil fuel consumed versus electricity generated) than CCGTs [7], the limitation in thermal inefficiency associated with daily start-ups and shutdowns of the steam turbine in a CSP plant [8], the lower cost of implementing a solar field in a existing CCGT than building an entire CSP plant [8], and the fact that operation and maintenance can be performed by the CCGT staff.

Different approaches and technologies are suitable for an ISCC power plant. However, the whole global installed ISCC capacity and most of the studies [8–10] are based on the PT-HTF technology. This is explained by its lower financial risk and the knowledge acquired in CSP plants with PT-HTF since the 1980s. Nevertheless, other possibilities arise depending on the working fluid, solar concentrating technology or the goal of integration. Regarding the working fluid, the direct steam generation technology applied to ISCCs is very promising [11–14] since it reduces the cost associated with the HTF and its intrinsic limitations in working fluid temperatures. Other working fluids such as the CO_2 have also been analyzed with parabolic troughs [15]. Regarding the method used to capture solar radiation, the solar tower technology has been analyzed with volumetric receivers using air as working fluid and transferring the heat into the Brayton cycle of the gas turbine [16–18]. The solar tower technology has also been studied in an ISCC power plant with HTF [19]. Linear Fresnel reflecting solar collectors have been considered in the potential hybridization with a CCGT [20]. Fresnel reflectors have also been analyzed with the aim to solve the air flow reduction problem caused by high inlet air temperatures, using the term *solar assisted combined cycle plant* [21]. These reflectors activate an absorption chiller that cools the inlet air. Another way to use the solar power consists of generating a syngas fuel from a chemical reaction using solar concentrated energy and mixing it with the original fuel in the combustor [22]. Solar steam can also be used for CO_2 capture in fossil fuel powered plants [22]. For a deep review on the status of the solar thermal and ISCC technologies the authors refer to Jamel et al. [23].

Fig. 1 represents a typical ISCC with PT-HTF. The solar field comprises different loops of parabolic trough solar collector assemblies (SCA) arranged in parallel, oriented on a North–South axis and therefore tracking the Sun from east to west. The heat transfer fluid temperature is regulated (to keep it constant and avoid fluid degradation) by controlling the speed of the main heat transfer fluid pump at the exit from the solar field. This heat is exchanged to generate steam in the solar steam generator and then injected into the medium pressure stage of the heat recovery steam generator (HRSG). ISCCs usually use solar thermal energy to displace latent heat in the HRSG, as a result of the similarities in the range of operating temperatures of the solar field (about 390 °C) and the medium-pressure stage of the steam turbine.

Many countries in the Middle East, the Mediterranean basin, and the southern region of the USA and elsewhere have installed a significant number of CCGTs in recent years, even though these areas experience high air temperatures over long periods, with the consequent negative impact on their electricity generation. For example, the installed CCGT capacity in mainland Spain is more than 25 GW, and most Spanish CCGTs experience direct normal irradiation in excess of 1700 kW h/m^2 year. This is enough irradiation to achieve a moderate levelized cost of electricity with PT-HTF, as is proved by Spain's total installed CSP capacity of 1950 MW at the end of 2012 [4], including some units with a similar range of irradiation. This means that there is enormous potential for improving CCGT efficiency and yield by means of hybridization with solar thermal energy [3,24].

Different assessments of the potential of ISCC have been proposed for individual CCGTs, such as the Yazd CCGT power plant [9,10,25] and the Hassi R'mel plant [26,27]. Some of these

Table 1
Global ISCC projects and their status.

Project	Country	Total capacity (MWe)	Solar capacity (MWe)	Status
MNGSEC	USA	1125	75	Operative since 2010
Archimede	Italy	750	5	Operative since 2010
Hassi R'mel	Algeria	150	25	Operative since 2011
Ain Beni Mathar	Morocco	470	20	Operative since 2011
Kuraymat	Egypt	140	20	In construction
Yazd	Iran	474	11	In construction
Victorville 2	USA	570	50	Under development
Palmdale (PHPP)	USA	573	50	Under development

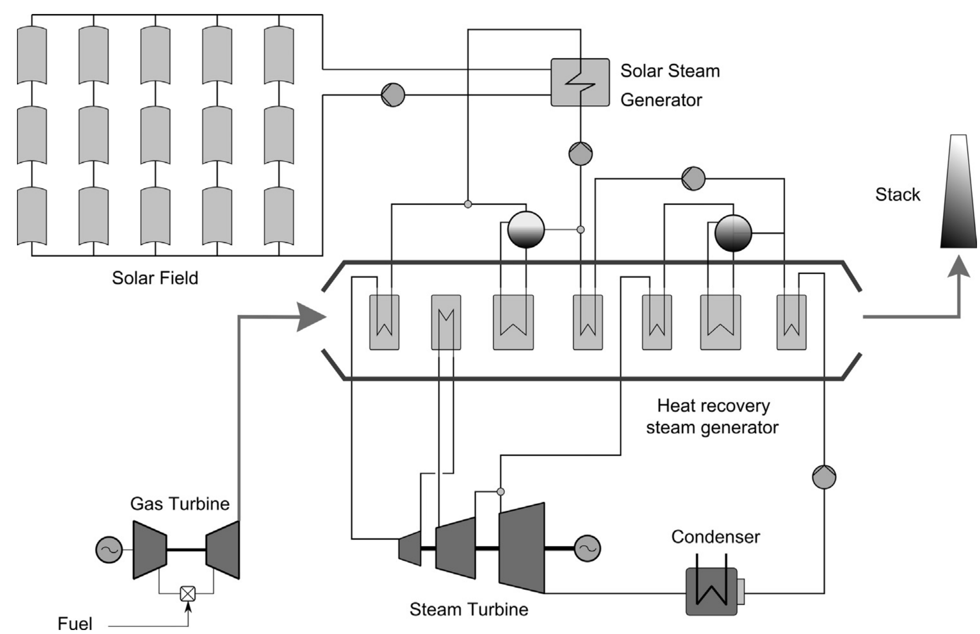


Fig. 1. ISCC scheme with solar field using PT-HTF technology.

assessments are based on increasing the steam turbine size by re-designing it, leading to greater solar integration.

However, there are no records on the impact of this technology on all the CCGTs in a country. The main objective of this paper is to assess the potential for integrating solar thermal energy into 51 CCGTs already operating in mainland Spain. The assessment is performed using different operation scenarios focused on increasing electricity production or the solar fraction and also scheduled to the typical CCGT operation hours in the Spanish electricity market.

An ISCC production model built in R open software is extensively described in terms of thermo-dynamical and solar field empirical equations (the code is freely available at https://github.com/feantot/ISCC) to enable the study to be repeated in other CCGTs. Finally, results are provided with different solar field configurations in terms of the number of loops of the solar field for each ISCC and scenario.

2. Data

This section is divided into Section 2.1, which deals with the process of selecting CCGTs in mainland Spain, and Section 2.2, which contains the meteorological information required to simulate the performance of the CCGTs and ISCCs.

2.1. CCGT data

The Spanish mainland electricity grid contains 51 CCGTs with a gross power output of 25,340 MW, out of a total installed capacity of 101,828 MW [28]. However, many of these CCGTs are not suitable for conversion to ISCC because of issues with the land available in their surroundings (the possible presence of inhabited areas and industrial zones, with the figure for this study set at a minimum of 12 ha) and the terrain (the range of elevations in the area is lower than the limit set, which is 20 m in this study). As a result, a visual inspection was performed, with visits to some CCGTs, and the Google Earth tool was also used to determine the ISCC-suitability of each CCGT. Table 2 shows the 30 CCGTs (17 different positions) selected (out of the original total of 51) as meeting the aforementioned conditions. The table also provides information regarding the gross power of the cycles and their gas and steam turbines.

2.2. Meteorological data

Once the suitable CCGTs have been selected, meteorological records are required to simulate CCGT and ISCC performance. To that end, the hourly direct normal irradiation (DNI) is calculated from the direct horizontal irradiation, dividing it by the cosine of the corresponding angle of incidence, from the Satellite Application Facility for Climate Monitoring (CM SAF) [29], a free-download satellite-derived database. The year 2005 is chosen as a representative year based on the DNI values in the positions of the CCGTs.

In addition, hourly meteorological datasets of air temperatures (T_a), relative humidity (Rh) and air pressure (p) are collated from records for 2005 from meteorological stations near each CCGT. The T_a and Rh datasets were freely obtained from the *Spanish Service of Information for Irrigation* (*SIAR*) [30], a body belonging to Spain's Ministry of Agriculture, Food and the Environment, except for CCGTs 29 and 30 (Tarragona Endesa and Tarragona Power), the datasets for which were obtained from the *Catalonian Meteorological Institute* (*MeteoCat*) [31]. Meteorological sensors are calibrated based on the TH-007 procedure of the Spanish Metrology Centre [32]. However, since SIAR and MeteoCat do not register p, the corresponding datasets were obtained from the *Spanish Meteorological Service* (*AEMET*) [33], from stations located at elevations similar to those of each CCGT. Fig. 2 shows the positions of the meteorological stations selected and their respective CCGTs. Table 2 shows the average values of the meteorological variables in 2005 for each CCGT.

3. Methodology

The methodology is proposed in two parts: Section 3.1 covers the production model and examines the main equations explaining the solar field and the performance of the turbines; Section 3.2 covers the operating scenarios, describing the modes of operation of the ISCCs. Fig. 3 shows the methodology proposed.

Table 2
CCGTs connected to the national grid in mainland Spain with information on latitude (Lat.), longitude (Lon.), elevation (Elev.), gross power (P), land available in the surroundings (Land), terrain suitable for the solar field (Rel.), gas turbine power rating (GT), steam turbine power rating (ST), annual direct normal irradiation (*DNI*) in kWh/m^2, average air temperature (T_a), average relative humidity (*Rh*) and average air pressure (*p*).

#	Name	Lat.	Lon.	Elev.	P	Land	Rel.	GT	ST	*DNI*	T_a	*Rh*	*p*
1	Aceca 3	39.9	-3.8	470	400	Yes	Yes	256	144	1784	14.7	54	957
2	Aceca 4	39.9	-3.8	470	374	Yes	Yes	240	134	1784	14.7	54	957
3	Algeciras 3CC	36.1	-5.3	13	821	Yes	Yes	562	259	1823	17.1	66	1015
–	Amorebieta	43.2	–2.7	123	749	No	No	–	–	–	–	–	–
4	Arcos 1	36.6	–5.8	177	396	Yes	Yes	253	143	1871	17.3	57	1015
5	Arcos 2	36.6	–5.8	177	379	Yes	Yes	243	136	1871	17.3	57	1015
6	Arcos 3	36.6	–5.8	177	823	Yes	Yes	529	294	1871	17.3	57	1015
7	Arrubal 1	42.4	–2.2	362	400	Yes	Yes	260	140	1330	12.7	67	976
8	Arrubal 2	42.4	–2.2	362	400	Yes	Yes	260	140	1330	12.7	67	976
–	Bahia Bizkaia	43.3	–3.1	6	800	No	No	–	–	–	–	–	–
–	Besos (3&4&5)	41.4	2.2	3	1692	No	Yes	–	–	–	–	–	–
9	C. Gibraltar 1	36.1	–5.4	17	400	Yes	Yes	260	140	1823	17.1	66	1015
10	C. Gibraltar 2	36.1	–5.4	17	400	Yes	Yes	260	140	1823	17.1	66	1015
–	Cartag. (1&2&3)	37.6	-0.9	10	1269	No	No	–	–	–	–	–	–
11	Castejon 1	42.2	–1.7	270	400	Yes	Yes	260	140	1297	13.1	70	977
12	Castejon 2	42.2	–1.7	270	400	Yes	Yes	260	140	1297	13.1	70	977
13	Castejon 3	42.2	–1.7	270	400	Yes	Yes	260	140	1297	13.1	70	977
14	Castellon 3	39.9	0.0	5	782	Yes	Yes	499	283	1618	15.9	65	1014
15	Castellon 4	39.9	0.0	5	839	Yes	Yes	534	305	1618	15.9	65	1014
16	Castelnou	41.2	–0.3	243	791	Yes	Yes	526	265	1634	14.3	61	988
17	Colon 4	37.2	–6.9	15	388	Yes	Yes	240	148	2136	16.3	70	1016
–	El Fang. (1&2&3)	37.5	–0.9	2	1219	No	No	–	–	–	–	–	–
18	Escatron 3	41.3	–0.3	131	804	Yes	Yes	539	265	1638	14.7	63	988
19	Escatron Peaker	41.3	–0.2	147	274	Yes	Yes	200	74	1620	14.7	63	988
–	Escombreras 6	37.6	–0.9	1	831	No	No	–	–	–	–	–	–
20	Malaga 1 CC	36.8	–4.6	75	430	Yes	Yes	280	150	1808	17.7	62	1017
21	Palos 1	37.2	–6.9	21	400	Yes	Yes	266	134	2146	16.3	70	1016
22	Palos 2	37.2	–6.9	21	400	Yes	Yes	266	134	2146	16.3	70	1016
23	Palos 3	37.2	–6.9	21	400	Yes	Yes	266	134	2146	16.3	70	1016
–	Plana Vent (1&2)	40.9	0.8	63	833	No	No	–	–	–	–	–	–
–	P. G. Rodr. 5	43.4	–7.9	344	849	No	No	–	–	–	–	–	–
–	P. Bna. (1 & 2)	41.3	2.2	49	848	No	No	–	–	–	–	–	–
–	Sabon 3	43.3	–8.5	20	389	No	No	–	–	–	–	–	–
24	Sagunto 1	39.6	–0.2	3	400	Yes	Yes	260	140	1538	17.3	62	1010
25	Sagunto 2	39.6	–0.2	3	400	Yes	Yes	260	140	1538	17.3	62	1010
26	Sagunto 3	39.6	–0.2	3	400	Yes	Yes	260	140	1538	17.3	62	1010
27	San Roque 1	36.2	–5.4	6	400	Yes	Yes	260	140	1846	17.1	66	1015
28	San Roque 2	36.2	–5.4	6	400	Yes	Yes	260	140	1846	17.1	66	1015
–	Santurce 4	43.3	–3.0	40	403	No	No	–	–	–	–	–	–
–	Soto Ribera (4&5)	43.3	–5.9	121	866	No	No	–	–	–	–	–	–
29	Tarrag. Endesa	41.1	1.2	15	400	Yes	Yes	260	140	1708	16.7	71	1009
30	Tarrag. Power	41.1	1.2	20	400	Yes	Yes	260	140	1704	16.7	71	1009

3.1. Production model

The production model is presented via the CCGT analysis (Section 3.1.1) and the solar field calculations (Section 3.1.2).

3.1.1. CCGT analysis

The influence of meteorological conditions is assessed based on the CCGT turbine performance, denoted as η_{meteo} operation in Fig. 3. The assessment is based on the ISO 2314:2009 design conditions, with $T_a=15\ ^\circ C$, $p=1013$ mb, and $Rh=60\%$.

Influence of T_a: The main factor affecting the performance of a CCGT is the inlet air temperature of the gas turbine (GT). This is because of its volumetric-machine behavior, which means that a GT always works with the same air volume. As a result, when T_a increases the mass flow entering the GT decreases (based on the law of ideal gases) and this is directly related to the energy generated by the CCGT.

Eqs. (1), 2) and (3) denote the relative power outputs (RPO) of GT, ST and CCGT, respectively, with T_a. These equations have been derived from [34–36] with the specifications in Table 3 for a 400 MW CCGT (similar to 25 from the 30 CCGT analyzed). The T_a affects not only the *mass flow* but also the specific energy consumed by the compressor, as a result of the variation in the pressure ratio between the turbine and the compressor (implying a net-energy yield loss):

$$RPO_{GT-T_a} = -0.005024 \cdot T_a + 1.07536 \quad (1)$$

$$RPO_{ST-T_a} = 6 \times 10^{-6} \cdot T_a^2 - 0.001579 \cdot T_a + 1.0224 \quad (2)$$

$$RPO_{CCGT-T_a} = 2.1 \times 10^{-6} \cdot T_a^2 - 0.00381 \cdot T_a + 1.056794 \quad (3)$$

Influence of p: The *p* is another factor affecting CCGT performance. A decrease in *p* has an effect similar to that of an increase in T_a, since the air becomes less dense and, consequently, *mass flow drops*. This affects the GT and ST power outputs, but not the efficiency, as the energy provided to the turbine, like the airflow, varies proportionally [34]. GTs are generally designed to produce their rated power output at the pressure conditions of each altitude, as *p* varies with altitude. Therefore, the only variation in the power output is produced by daily fluctuations in *p*, as per Eq. (4). The effect of *p* on ST performance is neglected:

$$RPO_{GT-p} = 1.08 \cdot \frac{p}{p_{design}} - 0.08 \quad (4)$$

where p_{design} is the pressure relative to each altitude, for which the gas turbine produces its rated nominal power output.

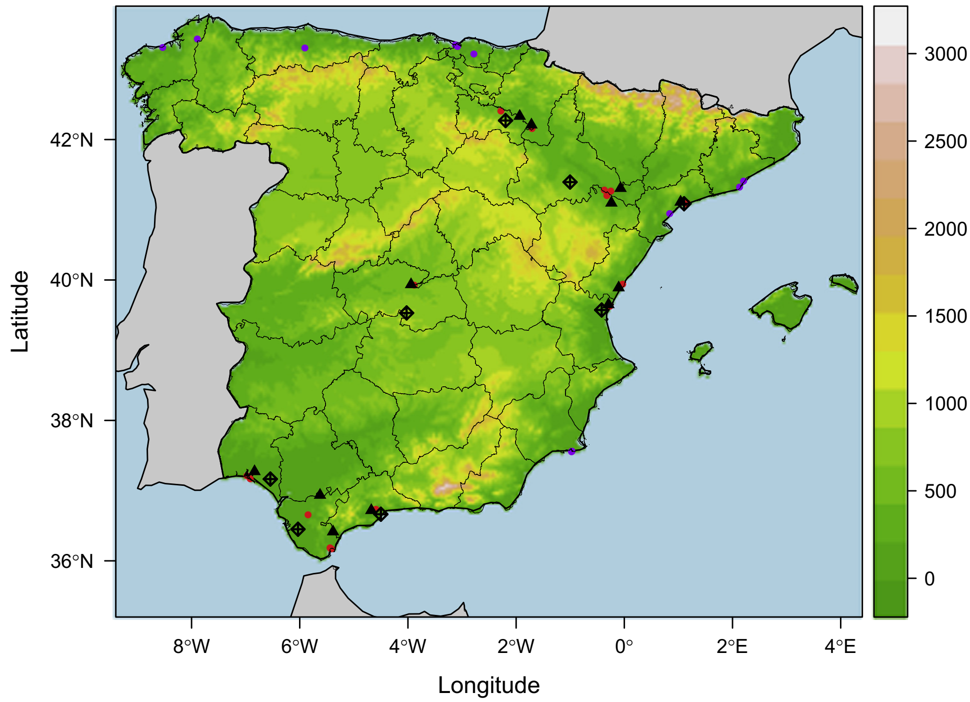


Fig. 2. Topographical map showing the CCGTs in mainland Spain. Red and purple points stand for CCGTs selected and rejected, respectively. Black triangles represent meteorological stations from which air temperatures and relative humidity are obtained and black rhomboids stand for meteorological stations measuring air pressure. (For interpretation of the references to color in this figure caption, the reader is referred to the web version of this paper.)

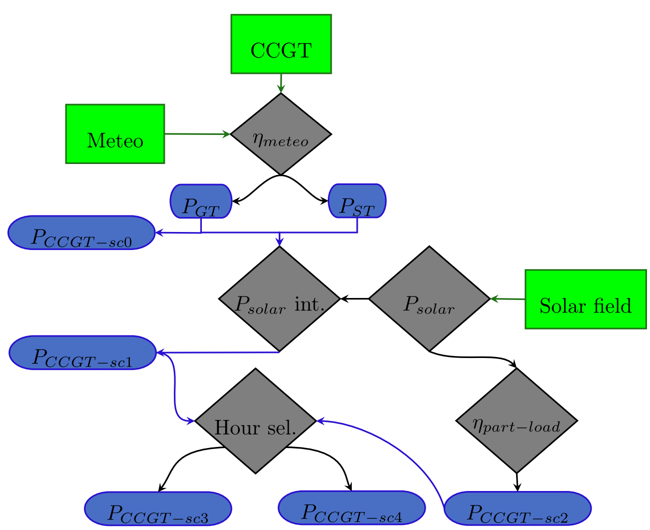


Fig. 3. Schematic diagram of the methodology proposed. Green rectangles stand for data sources, grey rhomboids for specific operations, and blue ellipses for results. (For interpretation of the references to color in this figure caption, the reader is referred to the web version of this paper.)

Influence of Rh: *Rh* has only a minor effect on CCGT performance. Nevertheless, a higher *Rh* in the air leads to a higher air enthalpy. Eq. (5) relates the RPO of the GT and *Rh*, the effect on the ST is disregarded [34]:

$$RPO_{GT-Rh} = 0.0116 \cdot Rh + 0.993 \quad (5)$$

Finally, the power output of the CCGT (in Fig. 3, $P_{CCGT-sc0}$) is obtained from the GT and ST power outputs (P_{GT} and P_{ST}).

3.1.2. Solar field analysis

Solar thermal production is approached by considering the specific DNI and the corresponding solar geometry for each CCGT.

Table 3
Technical specifications of the 400 MW CCGT selected.

Variable	Value
Natural gas LHV	39,900 kJ/kg
Nominal air volumetric flow	610 m^3/s
Gas temperature	25 °C
Nominal gas volumetric flow	20 kg/s
Compressor isentrophic efficiency	0.85
GT isentrophic efficiency	0.9

Table 4
Technical specifications of the solar field selected.

SCA length	99 m
SCAs per loop	4
Mirror cleanliness	97.0%
Transmissivity	95.5%
Reflectivity	94.0%
Interception factor	99.7%
Absorptivity	95.5%
Emittance	9.5%
Width	5.76 m
Focal distance	1.71 m
Opening area	545 m^2
Inlet HTF temperature	293 °C
Oulet HTF temperature	393 °C

The solar field is designed with LS-3 collectors, which have been extensively studied [10,25] and installed in commercial CSP plants [37]. Table 4 shows the technical specifications of the solar field selected with collectors oriented on a North–South axis. Some of the parameters of the solar field, such as the reflectivity, absorptivity and transmissivity, are provided by manufacturers for an incidence angle (φ) of 0° (Table 4). As a result, they must be corrected for other φ with Eq. (6) (valid for φ between 0° and 80°

for LS-3 collectors oriented on a North–South axis) [38]. In case of higher φ, $k(\varphi)$ is assumed to be null. This correction takes into account optic and geometric losses at the ends of the troughs:

$$k(\varphi) = 1 - 2.23073 \times 10^{-4} \cdot \varphi - 1.1 \times 10^{-4} \cdot \varphi^2 + 3.18596 \times 10^{-6} \cdot \varphi^3 - 4.85509 \times 10^{-8} \cdot \varphi^4 \quad (6)$$

Optical efficiency has to be considered to calculate the heat absorbed by the fluid, also modified with $k(\varphi)$:

$$\epsilon_{opt} = k(\varphi) \cdot \eta_{opt,0^\circ} \quad (7)$$

where $\eta_{opt,0^\circ}$ is the optical efficiency for an angle of incidence of 0° calculated with the following equation:

$$\eta_{opt,0^\circ} = \rho \cdot \gamma \cdot \tau \cdot \alpha \quad (8)$$

where ρ is the reflectivity, γ the interception factor, τ the transmissivity and α the absorptivity.

Because of φ, part of the sunlight is reflected out of the absorber tubes without transmitting its energy to the fluid. Eq. (9) takes into account this surface loss:

$$A_{loss} = b \cdot \left(d_f + \frac{b^2}{48 \cdot d_f} \right) \cdot \tan \varphi \quad (9)$$

where b is the collector width and d_f is the focal distance of LS-3.

From this point, the potential amount of energy transmitted to the collectors is calculated, from which different losses are later discounted:

$$P_{Q,sol \to collector} = A_{collector} \cdot DNI \cdot \cos \varphi \quad (10)$$

where $P_{Q,sol \to collector}$ is the energy radiated over the opening area of the collector ($A_{collector}$).

The fluid temperature is determined by the technical limitations of the absorber tube and thermal fluid (Therminol VP-1), which begins to chemically degrade at temperatures higher than 395 °C. For this reason, typical temperatures of 293 and 393 °C are selected at the entrance to and exit from the solar field, respectively. As a consequence of the high temperatures of the thermal fluid, a part of the heat is transmitted to the atmosphere through radiation losses [37]:

$$P_{Q,collector \to atm} = \left(0.00154 \cdot \Delta T^2 + 0.2021 \cdot \Delta T - 24.899 + \left[(0.0036 \cdot \Delta T^2 + 0.2029 \cdot \Delta T + 24.899) \left(\frac{E_d}{900} \cdot \cos \varphi \right) \right] \right) \cdot L \quad (11)$$

where ΔT is the difference between the temperature of the oil and the atmosphere and L is the longitude of the LS-3 trough.

Eventually, the thermal power transmitted by the collector to the working oil is obtained with the following equation (denoted as P_{solar} operation in Fig. 3):

$$P_{Q,collector \to fluid} = (A_c - A_{loss}) \cdot DNI \cdot \cos \varphi \cdot \eta_{opt,0^\circ} \cdot k(\varphi) \cdot F_e - P_{Q,collector \to atm} \quad (12)$$

where F_e is the collector fouling factor.

The efficiency of the steam generation process is assumed to be 93% [10] and the parasitic consumption of the solar field assumed to be 6% of the instantaneous solar power.

3.2. Scenarios of operation

The assessment is performed under five different ISCC scenarios based on the strategy in which solar thermal energy is injected. It is analyzed in a CCGT regular scenario, in order to better compare results.

3.2.1. Scenario 0

In this scenario, the ISCC is operated as a CCGT. As a result, no solar energy is used and the cycle works as usual. The gas turbine is operated under full load. This scenario is considered as a benchmark for scenarios 1 and 2.

3.2.2. Scenario 1

This operating mode has previously been considered as a *solar boosting* mode [5]. The GT is operated under full load and the steam from the solar input is used to increase the energy production when the CCGT production drops as a result of weather conditions. The usable solar power is calculated as the difference between the rated power output and the actual output. In this operating mode there can be a solar power excess, produced when the ST is running under full load, independently of whether this turbine is using solar-produced steam or not. This power excess is referred to as solar dumping and constitutes inefficiency in the ISCC. Solar dumping is usually avoided by taking solar collector assemblies out of focus, or stored using a thermal storage system [37].

3.2.3. Scenario 2

In this scenario 2, also denoted as *solar displacing* mode, all the steam generated by the solar field is injected into the ST. This operation mode involves reducing the load of the GT to adapt to the steam flow and, therefore, avoid solar dumping. The GT power is calculated as the rated power considering not only the atmospheric factors, as in the rest of the cases, but also the partial load yield loss.

3.2.4. Scenario 3

As a result of the Spanish regulatory framework, CCGTs are not priority facilities in the Spanish electricity grid (the base suppliers are nuclear, coal, hydro and special regime plants comprising renewables and cogeneration) so they normally operate with daily start-ups and shutdowns to meet peaks in demand. Fig. 4 shows the hourly power demand trend in Spain.

It can be derived from Fig. 4 that nights are off-peak hours, so CCGTs do not normally operate then. This may foster greater

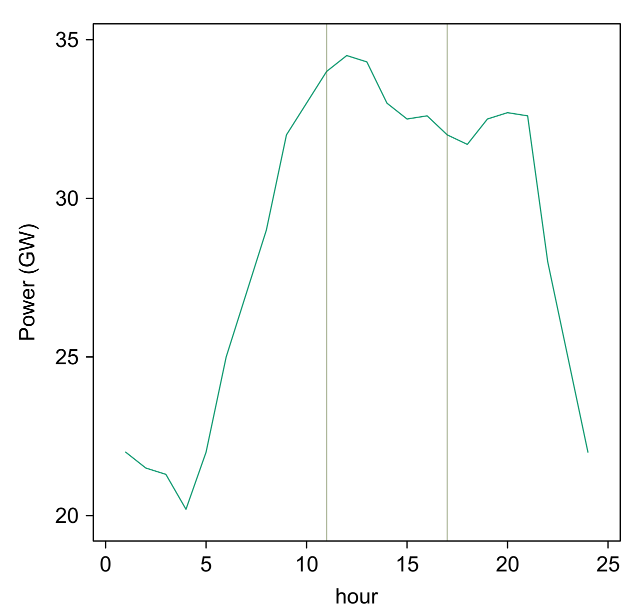


Fig. 4. Spanish electricity demand curve on a typical summer day.

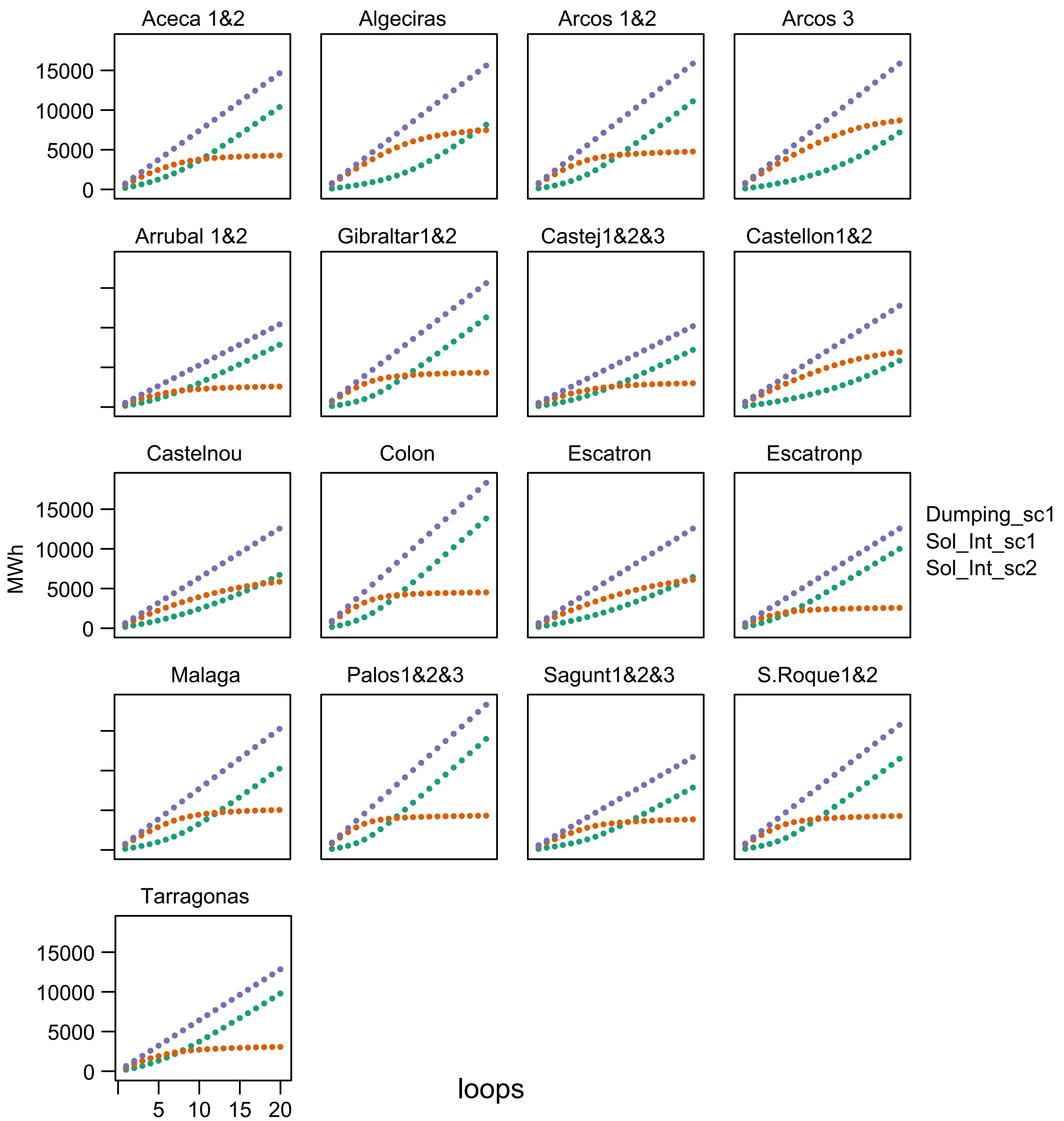


Fig. 5. Annual solar integration and dumping related to the number of loops of the solar field with scenarios 1 and 2.

integration of solar power, given that CCGTs work when solar radiation is available.

Scenario 3 seeks to fit better into the performance of the Spanish electrical grid. For this reason, CCGTs are considered to generate only in peak hours, from 11:00 to 17:00 (local time), a period when high solar radiation coincides with high demand for power.

The operation and calculation mode are the same as for scenario 1; during the time considered the gas turbine runs under full load. The period considered is not longer because there is less solar radiation in the early and late hours of the day and results similar to those for scenario 1 would be obtained. In this scenario a high percentage of solar integration is sought. It must also be said that in summer months the peak demand hours occur in the early afternoon, coinciding with the hours when the temperature is highest, which is why CCGT production drops.

3.2.5. *Scenario 4*

This scenario follows the same pattern of hours as scenario 3 (11:00–17:00) but with the same operating conditions as scenario 2, i.e. all the steam produced in the solar field is used, and the load of the GT has to be reduced as a result, to adapt to the steam flow.

3.2.6. *Scenario 5*

The ISCC is operated as a CCGT, similar to scenario 0 but for the same pattern of hours as in scenarios 3 and 4.

3.3. *Software*

The methodology explained in this paper is implemented using the free software `R` [39] and several contributed packages: `solaR` [40] for solar geometry analysis, `raster` [41] for spatial data

manipulation and analysis and `rasterVis` [42] for spatial data visualization methods.

4. Results and discussion

The performance of ISCCs is approached via a *local analysis* (Section 4.1), in which different variables such as the increase in efficiency, solar integration and dumping are analyzed and via an *overall analysis* (Section 4.2) in which those variables are analyzed overall in mainland Spain.

4.1. Local analysis

The methodology proposed above is applied to the 30 CCGTs suitable for conversion to ISCCs with different solar field sizes, ranging between 1 and 20 LS3-loops. Fig. 5 shows the annual potential solar integration with scenarios 1 and 2 and the solar dumping with scenario 1, all related to the number of loops. The greatest increase in solar integration in scenario 1 takes place in the first number of loops, when there is still a potential improvement in ST performance. Subsequently, solar integration stabilizes since the ST cannot absorb any more solar-produced steam, and it is at that point where dumping begins to increase in proportion to the growth of the solar field. Solar integration follows an asymptotic curve with scenario 1 (solar boosting mode) while solar dumping increases significantly with the number of loops. In the case of 400 MW power plants, solar integration tends to stabilize in scenario 1 at a solar field size of 7–10 loops, with the most significant increase being found in up to five loops.

Solar integration in scenario 2 varies in proportion to the size of the solar field, as the ST absorbs all the steam produced. It can be obtained as the addition of solar integration in scenario 1 with dumping. As a result, there is no dumping in scenario 2 since all the solar thermal energy is injected into the ST by part-loading the GT. This graphic shows the importance of choosing the correct solar field size, since a bigger solar field would produce more solar steam than necessary and that excess would become an indicator of ISCC inefficiency.

Table 5
Number of loops in the solar field for each CCGT to obtain R of 30%, 50%, 80% and 100%.

%/#	1,2	3	4,5	6	7,8	9,10	11,12,13	14,15	16	17	18	19	20	21,22,23	24,25,26	27,28	29,30
30%	1	9	4	9	1	5	1	6	1	4	1	1	4	5	3	4	1
50%	5	13	7	15	4	7	5	14	8	6	9	3	8	6	8	7	3
80%	9	17	10	20	7	9	9	20	15	8	16	6	11	8	11	9	7
100%	11	19	11	> 20	8	11	11	> 20	18	10	20	7	13	9	13	10	8

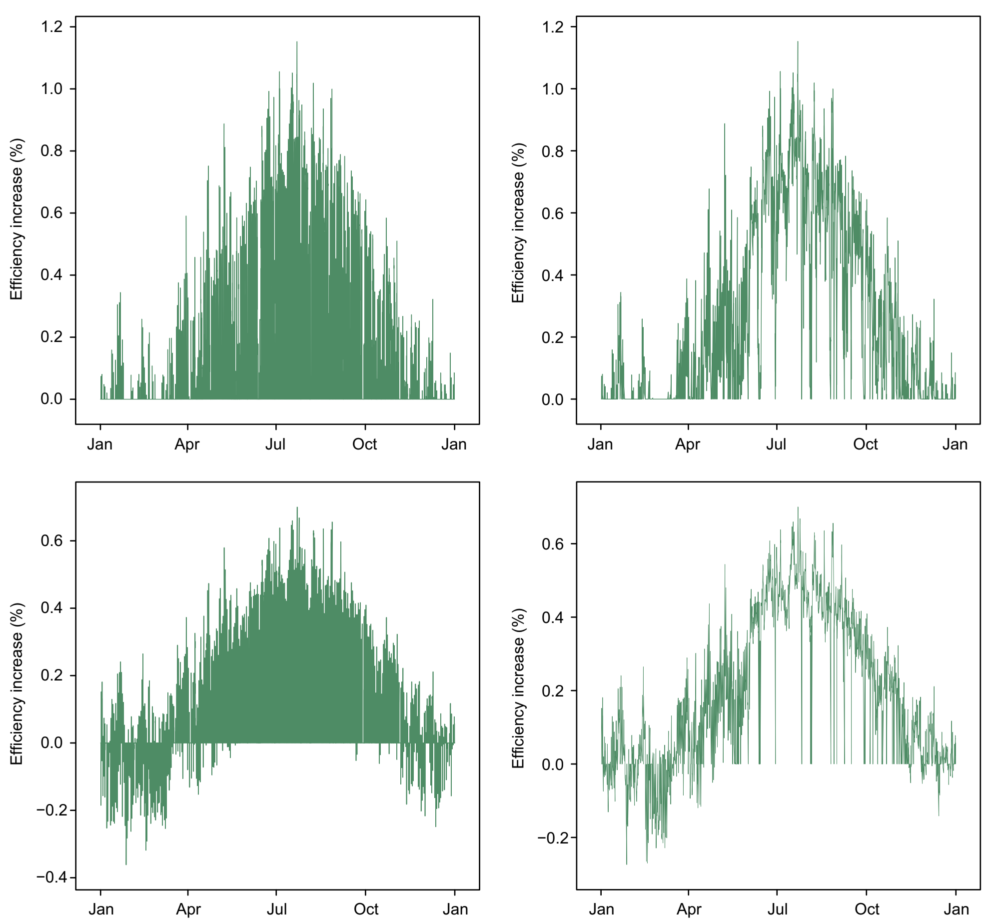


Fig. 6. Efficiency increase in the Malaga CCGT with a 10-loop solar field in scenarios 1 (up left figure), 3 (up right figure), 2 (down left figure) and 4 (down right figure). (For interpretation of the references to color in this figure caption, the reader is referred to the web version of this paper.)

To assess the performance of scenario 1, the dumping ratio (R) is defined as the ratio of usable solar energy to dumping under scenario 1. Table 5 shows the minimum number of loops that gives R values of 30%, 50%, 80% and 100%. As can be deduced from this table, the location of the CCGTs significantly affects the number of loops. The R ratio is defined to show the importance of dumping when scenario 1 is considered. For instance, for similar 400 MW CCGTs in Malaga and Arrubal 1&2, 11 and 7 loops, respectively, would be necessary to account for an R of 80%.

To better describe ISCC performance, the efficiency increase related to the base scenarios (0 and 5) is assessed. This efficiency increase is calculated with the following equation:

$$\mu = P_{iscc_s}/P_s - P_{ccgt_{base}}/P_{base} \qquad (13)$$

where P_{iscc_s} is the ISCC power with scenario s, $P_{ccgt_{base}}$ is the reference CCGT power and P_s and P_{base} are the low heating power of natural gas injected into the GT in the s and $base$ scenarios.

As an example, Fig. 6 shows the efficiency increase with scenarios 1, 2, 3 and 4 at the Malaga CCGT with a 10-loop solar field. Malaga is in the South of Spain, with mild winters and hot summers. Similar results to those of the Malaga CCGT are obtained in the other 400 MW CCGTs.

Scenarios 1 and 3 give rise to an efficiency increase of 0.5% from June to October, and as much as 0.7% in some summer months when the T_a is high and high DNI is also available. In winter, when atmospheric conditions are more favorable to CCGT performance, the increase in overall efficiency is very small. In contrast, working in winter months with scenarios 2 and 4 there is a decrease in efficiency because the GT has to reduce its load to absorb the solar-produced steam in the ST, thus worsening the performance of the GT when it should be working with a high level of efficiency. Moreover, the efficiency increase in summer is not as great as that obtained in scenario 1, as it exceeds 0.5% on only a very few days. It can be concluded from this figure that scenarios 2 and 4 generate an efficiency loss not only in the winter but also during the rest of the year when compared with scenarios 1 and 3. As a result, most of the ISCCs in operation have been designed with oversized STs so as to avoid part-load operation of the GT and operate it always under full load [10].

Fig. 7 describes the performance of the Malaga CCGT on 28 June 2005. This date was chosen as an example of a typical summer day at this location. The graph shows the intraday-trend working under scenarios 1 and 2 with a 10-loop solar field. In these conditions, the CCGT behaves out of line with its design conditions and the performance worsens. The yellow curve shows the power output, revealing that up to 20 MW is lost in the most unfavorable conditions. An increase of up to 7 MW and 2.5 MW would be possible with scenarios 1 and 2, respectively, when atmospheric conditions are at their worst, and solar dumping is very low.

The conversion of Spanish CCGTs into ISCCs depends on the existing and very changing electric regulatory frame during the last years. This frame prioritizes the access to other technologies (pure renewable energy technologies, hydro, cogeneration and nuclear) respect to CCGTs, which in many cases are operated less than 1000 h per year [28], significantly lower than their expected generation. As a result, the conversion of these CCGTs into ISCC should be accompanied with a more stable regulatory frame and with initiatives promoting ISCCs.

4.2. Total analysis

Table 6 shows the cumulative performance of the ISCCs under scenarios 1 and 2 in mainland Spain. Scenario 2 generates a higher net-yield than scenario 1 for solar fields up to three loops. This is explained by the fact that efficiency increase with scenario 2 is higher than the dumping associated with scenario 1 for these solar field sizes. However, for larger numbers of loops scenario 1 outperforms scenario 2 as a result of the part-load operation of the GTs. It is noteworthy that for $>15-$loop solar field sizes a yield-loss is observed: yield is indeed lower than in the base case scenario 0. In overall terms, the R is higher than 100% for solar field sizes above 10 loops.

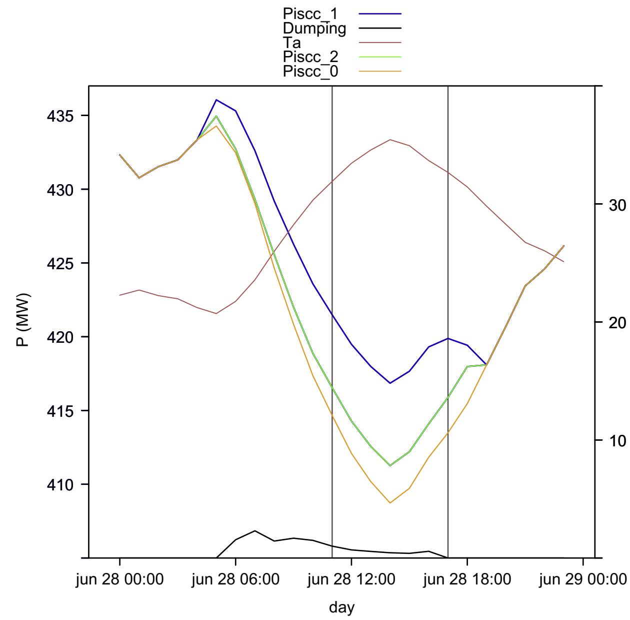


Fig. 7. Assessment of the Malaga ISCC with a 10-loop solar field on a particular summer day. Both T_a and solar dumping use the right y-axis. Vertical lines represent the hour range for scenarios 5, 3 and 4 (11:00–17:00). (For interpretation of the references to color in this figure caption, the reader is referred to the web version of this paper.)

The fictitious savings in CO_2 emissions (SE) are calculated with the general conversion for CCGTs of 0.372 kg CO_2/kWh [43], significantly lower than for CSP plants [44]. This means that for a 10-loop solar field the figures would be 41.1 and 77.9 kton CO_2/year for scenarios 1 and 2, respectively. It must also be considered that the yield in scenario 2 is lower than in scenario 1 for the same number of loops.

Similar results are obtained with scenarios 3 and 4, as shown in Table 7. Scenario 4 provides higher P_{iscc} than scenario 3 for solar fields up to two loops and lower than scenario 5 for solar field sizes greater than 17 loops. R is higher than 100% for solar field sizes above 12 loops, 2 more than in scenario 1, as a consequence of the hour discretization.

The overall solar power with a 10-loop solar field would be in the range of 110.5 GWh/year in scenario 1, while in scenario 2 it would be 209.3 GWh/year, generating a lower P_{iscc}. Nevertheless, considering scenarios 3 and 4, the P_s would be in the range of 77.1 and 135.7 GWh/year with similar solar field sizes. SE_3 and SE_4 would be 28.7 and 50.5 kton CO_2/year in a 10-loop solar field.

5. Conclusions

CCGTs are a more efficient, less polluting way of producing electric energy than coal-fired, fuel-oil-fired and other plants, but their performance is closely linked to the atmospheric conditions in each place and at each time. As a result, periods of high air temperatures (the main factor affecting production and performance) normally coincide with those when there is more direct normal irradiation; it becomes possible to integrate steam produced by solar thermal collectors to alleviate the production drop in CCGTs. These new plants, called ISCCs, combine CCGT

Table 6
Total results expressed as yield-annual sums against the number of loops in the solar field for scenarios 0, 1 and 2. Units are TWh/year, except for $P_{s,1}$, D_1 and $P_{s,2}$, which are GWh/year. $P_{ccgt,x}$, $P_{gt,x}$, $P_{st,x}$ and $P_{s,x}$ stand for the annual yield of the CCGT, GT, ST and solar yield in scenarios *x*. D_1 stands for the annual dumped energy with scenario 1. SE_1 and SE_2 represent the savings in CO_2 emissions in kton.

Loops	$P_{ccgt,0}$	$P_{gt,0}$	$P_{st,0}$	$P_{iscc,1}$	$P_{st,1}$	$P_{s,1}$	D_1	SE_1	$P_{iscc,2}$	$P_{gt,2}$	$P_{st,2}$	$P_{s,2}$	SE_2
1	127.4	82.9	44.51	127.45	44.53	16.9	4.0	6.3	127.49	82.86	44.63	20.9	7.8
2	127.4	82.9	44.51	127.48	44.54	33.0	8.9	12.3	127.49	82.85	44.63	41.9	15.6
3	127.4	82.9	44.51	127.51	44.56	48.0	14.7	17.9	127.48	82.85	44.63	62.8	23.4
4	127.4	82.9	44.51	127.54	44.57	61.8	21.9	23.0	127.47	82.84	44.63	83.7	31.1
5	127.4	82.9	44.51	127.56	44.59	74.0	30.6	27.5	127.47	82.84	44.63	104.6	38.9
6	127.4	82.9	44.51	127.58	44.60	84.4	41.1	31.4	127.46	82.83	44.63	125.6	46.7
7	127.4	82.9	44.51	127.60	44.61	93.1	53.4	34.6	127.46	82.83	44.63	146.5	54.5
8	127.4	82.9	44.51	127.61	44.61	100.1	67.3	37.2	127.45	82.82	44.63	167.4	62.3
9	127.4	82.9	44.51	127.62	44.62	105.8	82.6	39.4	127.44	82.81	44.63	188.3	70.0
10	127.4	82.9	44.51	127.64	44.62	110.5	98.8	41.1	127.44	82.81	44.63	209.3	77.9
11	127.4	82.9	44.51	127.65	44.63	114.4	115.7	42.6	127.43	82.80	44.63	230.2	85.6
12	127.4	82.9	44.51	127.66	44.63	117.8	133.3	43.8	127.42	82.79	44.63	251.1	93.4
13	127.4	82.9	44.51	127.66	44.63	120.8	151.2	44.9	127.42	82.79	44.63	272.0	97.5
14	127.4	82.9	44.51	127.67	44.64	123.4	169.6	45.9	127.41	82.78	44.63	293.0	109.0
15	127.4	82.9	44.51	127.67	44.64	125.6	188.3	46.7	127.40	82.77	44.63	313.9	116.8
16	127.4	82.9	44.51	127.67	44.64	127.6	207.2	47.5	127.40	82.77	44.63	334.8	124.5
17	127.4	82.9	44.51	127.68	44.64	129.3	226.5	48.1	127.39	82.76	44.63	355.7	132.3
18	127.4	82.9	44.51	127.68	44.64	130.8	245.9	48.7	127.38	82.75	44.63	376.7	140.1
19	127.4	82.9	44.51	127.68	44.64	132.1	265.5	49.1	127.37	82.74	44.63	397.6	147.9
20	127.4	82.9	44.51	127.68	44.65	133.3	285.2	49.6	127.37	82.74	44.63	418.5	155.7

Table 7
Total results expressed as yield-annual sums against the number of loops in the solar field for scenarios 5, 3 and 4. Units are in TWh/year, except for $P_{s,3}$, D_3 and $P_{s,4}$, which are in GWh/year. $P_{ccgt,x}$, $P_{gt,x}$, $P_{st,x}$ and $P_{s,x}$ stand for the annual yield of the CCGT, GT, ST and solar yield in scenarios *x*. D_3 stands for the annual dumped energy with scenario 3. SE_3 and SE_4 represent the savings in CO_2 emissions in kton.

Loops	$P_{ccgt,5}$	$P_{gt,5}$	$P_{st,5}$	$P_{iscc,3}$	$P_{st,3}$	$P_{s,3}$	D_3	SE_3	$P_{iscc,4}$	$P_{gt,4}$	$P_{st,4}$	$P_{s,4}$	SE_4
1	36.49	23.59	12.90	36.51	12.91	11.5	2.1	4.3	36.55	23.56	12.99	13.6	5.1
2	36.49	23.59	12.90	36.53	12.93	22.4	4.7	8.3	36.54	23.56	12.99	27.1	10.1
3	36.49	23.59	12.90	36.55	12.94	32.8	7.9	12.2	36.54	23.55	12.99	40.7	15.1
4	36.49	23.59	12.90	36.57	12.95	42.4	11.9	15.8	36.54	23.55	12.99	54.3	20.2
5	36.49	23.59	12.90	36.59	12.95	51.0	16.8	19.0	36.54	23.55	12.99	67.8	25.2
6	36.49	23.59	12.90	36.60	12.96	58.5	22.9	21.8	36.53	23.54	12.99	81.4	30.3
7	36.49	23.59	12.90	36.61	12.96	64.8	30.2	24.1	36.53	23.54	12.99	95.0	35.3
8	36.49	23.59	12.90	36.63	12.97	69.8	38.8	26.0	36.52	23.53	12.99	108.6	40.4
9	36.49	23.59	12.90	36.64	12.98	73.8	48.3	27.5	36.52	23.53	12.99	122.1	45.4
10	36.49	23.59	12.90	36.64	12.98	77.1	58.6	28.7	36.52	23.52	12.99	135.7	50.5
11	36.49	23.59	12.90	36.65	12.98	79.9	69.4	29.7	36.51	23.52	12.99	149.3	55.5
12	36.49	23.59	12.90	36.65	12.98	82.2	80.6	30.6	36.51	23.52	12.99	162.8	60.6
13	36.49	23.59	12.90	36.66	12.99	84.3	92.1	31.4	36.50	23.51	12.99	176.4	65.6
14	36.49	23.59	12.90	36.66	12.99	86.1	103.9	32.0	36.50	23.51	12.99	190.0	70.7
15	36.49	23.59	12.90	36.66	12.99	87.6	115.9	32.6	36.49	23.50	12.99	203.5	75.7
16	36.49	23.59	12.90	36.67	12.99	89.0	128.1	33.1	36.49	23.50	12.99	217.1	80.8
17	36.49	23.59	12.90	36.67	12.99	90.2	140.5	33.6	36.48	23.49	12.99	230.7	85.8
18	36.49	23.59	12.90	36.67	12.99	91.2	153.1	33.9	36.48	23.49	12.99	244.3	90.9
19	36.49	23.59	12.90	36.67	12.99	92.0	165.8	34.2	36.47	23.48	12.99	257.8	95.9
20	36.49	23.59	12.90	36.67	12.99	92.8	178.6	34.5	36.47	23.48	12.99	271.4	101.0

components with a solar collector field, improving cycle performance when working on out-of-design conditions.

Throughout the production model proposed, atmospheric and geographic characteristics have been analyzed to establish the potential improvement in output in CCGTs in mainland Spain. Geographical restrictions, such as land area and terrain, limit the number of CCGTs potentially suitable for hybridization to 30 out of the initial 51. Different scenarios have been analyzed depending on whether the priority is for solar integration (scenarios 2 and 4) or yield increment (scenarios 1 and 3), and also depending on the operating time: continuous operation (scenarios 1 and 2) and operation adapted to the Spanish peak demand curve (scenarios 3 and 4).

In scenarios 1 and 3, solar-produced steam boosts the ST up to full-load operation without interfering with GT performance. These scenarios offer a simpler way to operate an ISCC, since plant managers do not need to adapt GT to the solar output moment by moment. However, as solar field size grows there is an increase in solar dumping. The solar field size must therefore be designed specifically for each CCGT. Nevertheless, this dumping also provides an opportunity for solar thermal storage, cogeneration and parasitic thermal consumption within the CCGT. The R ratio is defined to better understand the link between solar integration and dumping. In most of the 400 MW CCGTs analyzed, an R of 80% is achieved with a solar field with fewer than 10 loops. It is observed that the greatest increase in solar contribution is located within the first few loops, up to 5. From 8 to 10 onwards the usable output hardly increases since the ST is not capable of absorbing any more solar-produced steam. It has been proved that it is possible to achieve efficiency increments in the range of 0.6–1% during daylight hours between May and October with 10-loop solar fields in 400 MW CCGTs.

Scenarios 2 and 4, which prioritize solar-produced steam integration instead of CCGT production, reduce the cycle efficiency in winter months, since part-load operation of the GT is less

efficient. During the summer months, the efficiency increase is in the range of 0.4–0.6%, i.e. lower than in scenarios 1 and 3 for part-load operation of the GT. Not only is the efficiency increase lower but so is the total yield. The operation of ISCCs under these scenarios is more complex, since GT load must be instantaneously adapted to the solar field output, which depends on the changing meteorology. However, in these scenarios no solar dumping is generated.

Results are presented locally and overall for mainland Spain. It would be possible to increase overall CCGT output by 110.5 and 77.1 GWh/year via solar integration in scenarios 1 and 3, respectively, considering solar field sizes of 10-loops. It would also be possible to save 41.1 and 28.7 kton CO_2/year in the same conditions.

Great potential for solar integration has been found to exist in Spanish CCGTs, especially in southern Spain. This provides an enormous opportunity to improve yield and efficiency in peak periods and reduce CO_2 emissions. The conversion of existing CCGTs in Spain to ISCCs presents some benefits: increasing generation in peak consumption periods (when electricity price is higher) and also the overall efficiency of the cycle, lowering the levelized cost of solar electricity (since many of the CCGT components are shared) when compared with pure CSP plants. In addition, there might be other benefits associated of government incentives based on feed in tariffs or priority access to the electricity market.

The code in `R` language is freely available at https://github.com/feantot/ISCC as Supplementary material, to help to replicate the hybridization assessment with other CCGTs.

Acknowledgments

This work has been partially financed by a project of the Instituto de Estudios Riojanos (IER, Spain). F. Antonanzas-Torres has a fellowship FPI at University of La Rioja, Spain.

References

[1] Zhanga HL, Baeyens J, Degrève J, Cacères G. Concentrated solar power plants: review and design methodology. Renew Sustain Energy Rev 2013;22:466–81.
[2] Peterseim JH, White S, Tadros A, Hellwig U. Concentrated solar power hybrid plants, which technologies are best suited for hybridisation? Renew Energy 2013;57:520–32.
[3] Jablonski S, Tarhini M, Touati M, Gonzalez Garcia D, Alario J. The Mediterranean solar plan: project proposals for renewable energy in the Mediterranean partner countries region. Energy Policy 2012;44:291–300.
[4] Renewables 2013 global status report. REN21, renewable energy policy network for the 21st century. URL 〈http://www.ren21.net/Portals/0/documents/Resources/GSR/2013/GSR2013_lowres.pdf〉.
[5] Antonanzas-Torres F, Sodupe E, Fernandez R, Sanz A, Martinez-de-Pison FJ. Technical feasibility assessment of integrated solar combined cycle power plants in Ciudad Real (Spain) and Las Vegas (USA). In: Proceedings of the 16th international congress on project engineering, Valencia, Spain; 2012.
[6] National Renewable Energy Laboratory (NREL). URL 〈www.nrel.gov/csp/solarpaces/〉.
[7] Derbal-Mokrane H, Bouaichaoui S, Gharbi NE, Belhamel M, Benzaoui A. Modeling and numerical simulation of an integrated solar combined cycle system in Algeria. Proc Eng 2012;33:199–208.
[8] Dersch J, Geyer M, Herrmann U, Jones SA, Kelly B, Kistner R, et al. Trough integration into power plants—a study on the performance and economy of integrated solar combined cycle systems. Energy 2004;29:947–59.
[9] Hosseini R, Soltani M, Valizadeh G. Technical and economic assessment of the integrated solar combined cycle power plants in Iran. Renew Energy 2005;30:1541–55.
[10] Baghernejad A, Yaghoubi M. Exergy analysis of an integrated solar combined cycle system. Renew Energy 2010;35:2157–64.
[11] Nezammahalleh H, Farhadi F, Tanhaemami M. Conceptual design and techno-economic assessment of integrated solar combined cycle system with DSG technology. Solar Energy 2010;84:1696–705.
[12] Li Y, Yang Y. Thermodynamic analysis of a novel integrated solar combined cycle. Appl Energy 2014;122:133–42.
[13] El-Sayed MAH. Solar supported steam production for power generation in Egypt. Energy Policy 2005;33:1251–9.
[14] Rovira A, Montes MJ, Varela F, Gil M. Comparison of heat transfer fluid and direct steam generation technologies for integrated solar combined cycles. Appl Thermal Eng 2013;52:264–74.
[15] Cau G, Cocco D, Tola V. Performance and cost assessment of integrated solar combined cycle systems (ISCCSs) using CO_2 as heat transfer fluid. Solar Energy 2012;86:2975–85.
[16] Spelling J, Favrat D, Martin A, Augsburger G. Thermoeconomic optimization of a combined-cycle solar tower power plant. Energy 2012;41:113–20.
[17] Kribus A, Zaibel R, Carey D, Segal A, Karni J. A solar-driven combined cycle power plant. Solar Energy 1998;62(2):121–9.
[18] Heide S, Gampu U, Orth U, Beukenberg M, Gericke B, Freimark M, et al. Design and operational aspects of gas and steam turbines for the novel solar hybrid combined cycle SHCC. In: ASME conference proceedings; 2010. p. 465–74.
[19] Franchini G, Perdichizzi A, Ravelli S, Barigozzi G. A comparative study between parabolic trough and solar tower technologies in solar rankine cycle and integrated solar combined cycle plants. Solar Energy 2013;98:302–14.
[20] Reddy VS, Kaushik SC, Tyagi SK. Exergetic analysis of solar concentrator aided natural gas fired combined cycle power plant. Renew Energy 2012;39:114–25.
[21] Popov D. Innovative solar augmentation of gas turbine combined cycle plants. Appl Thermal Eng 2014;64:40–50.
[22] Ordorica G, Delgado Vidal A, Fernandez Garcia A. Novel integration options of concentrating solar thermal technology with fossil-fuelled and CO_2 capture processes. Energy Proc 2011;4:809–16.
[23] Jamel MS, Abd Rahman A, Shamsuddin AH. Advances in the integration of solar thermal energy with conventional and non-conventional power plants. Renew Sustain Energy Rev 2013;20:71–81.
[24] Tsikalakis A, Tomtsi T, Hatziargyriou ND, Poullikkas A, Malamatenios Ch, Giakoumelos E, et al. Review of best practices of solar electricity resources applications in selected Middle East and North Africa (MENA) countries. Renew Sustain Energy Rev 2011;15(6):2838–49.
[25] Baghernejad A, Yaghoubi M. Exergoeconomic analysis and optimization of an integrated solar combined cycle system (ISCCS) using genetic algorithm. Energy Convers Manag 2011;52:2193–203.
[26] Boukelia TE, Mecibah M-S. Parabolic trough solar thermal power plant: potential, and projects development in Algeria. Renew Sustain Energy Rev 2013;21:288–97.
[27] Behar O, Kellaf A, Mohamed K, Belhamel M. Instantaneous performance of the first integrated solar combined cycle system in Algeria. Energy Proc 2011;6:185–93.
[28] Red Eléctrica de España Informe; 2012. URL 〈www.ree.es/sistema_electrico/informeSEE.asp〉.
[29] Climate Monitoring Satellite Application Facility. URL 〈www.cmsaf.eu〉.
[30] Servicio de Información Agroclimática del Regadío. URL 〈eportal.magrama.gob.es/websiar/Inicio.aspx〉.
[31] Servei Meteorològic de Catalunya. URL 〈http://www.meteo.cat/servmet/index.html〉.
[32] Spanish Centre of Metrology (CEM) URL 〈www.cem.es〉.
[33] Agencia Estatal de Meteorología. URL 〈www.aemet.es〉.
[34] Kehlhofer R, Hannemann F, Stirnimann F, Rukes B. Combined-cycle gas and steam turbine power plants. 3rd ed.. Tulsa, OK: PennWell; 2009.
[35] Siemens. URL 〈www.energy.siemens.com/hq/en/fossil-power-generation/gas-turbines/〉.
[36] Ponce Arrieta FR, Silva Lora EE. Influence of ambient temperature on combined-cycle power-plant performance. Appl Energy 2005;80:261–72.
[37] Fernández-García A, Zarza E, Valenzuela L, Pérez M. Parabolic-trough solar collectors and their applications. Renew Sustain Energy Rev 2010;14:1695–721.
[38] González E, Zarzaand E, Yebra L. Yebra,Determinación del modificador por ángulo de incidencia de un colector solar LS-3, incluyendo las pérdidas geométricas por final de colector. Informe técnico DISS-SC-SF-30. Almería, España, Plataforma Solar de Almería; 2001.
[39] R Development Core Team, R: a language and environment for statistical computing. R Foundation for Statistical Computing, Vienna, Austria; 2012. ISBN 3-900051-07-0. URL 〈http://www.R-project.org〉.
[40] Perpiñán-Lamigueiro O. `solaR`: solar radiation and photovoltaic systems with R. J Stat Softw 2012;50(9):1–32 URL 〈www.jstatsoft.org/v50/i09〉.
[41] Hijmans RJ, van Etten J. `raster`: geographic analysis and modeling with raster data, r package version 1.9-82; 2012. URL 〈http://cran:.R.R-project.org/package=raster〉.
[42] Perpinan O, Hijmans R. rasterVis: visualization methods for the raster package, r package version 0.10-9; 2012. URL 〈http://cran:.R.R-project.org/package=rasterVis〉.
[43] Instituto de Diversificación y Ahorro de la Energía. Plan de Energías Renovables 2005–2010. p. 351. URL 〈http://www.idae.es/index.php/mod.documentos/mem.descarga?file=/documentos_PER_2005-2010_8_de_gosto-2005_Completo.(modificacionpag_63)_Copia_2_301254a0.pdf〉.
[44] Chen GQ, Yang Q, Zhao YH, Wang ZF. Nonrenewable energy cost and greenhouse gas emissions of a 1.5 MAW solar power tower plant in China. Renew Sustain Energy Rev 2011;15:1961–7.